Prediction of transmission loss of double panels with a patch-mobility method

Jean-Daniel Chazot[a] and Jean-Louis Guyader
Laboratoire Vibrations Acoustique de l'INSA de Lyon, 25 bis avenue Jean Capelle, 69621 Villeurbanne Cedex, France

(Received 21 April 2006; revised 20 October 2006; accepted 20 October 2006)

Sound transmission loss through double panels is studied with a patch-mobility approach. An overview of the method is given with details on acoustic and structural patch mobilities. Plate excitation is characterized by blocked patch pressures that take into account room geometry and source location. Hence, panel patch velocities before coupling can be determined and used as excitation in the mobility model. Then a convergence criterion of the model is given. Finally, transmission loss predicted with a patch-mobility method is compared with measurements.
 [DOI: 10.1121/1.2395920]

PACS number(s): 43.55.Rg [NX] Pages: 267–278

I. INTRODUCTION

The first studies on sound transmission were done using unbounded plates excited by plane waves. Cremer's[1] and London's works on single panels[2] and on double panels[3] enabled us to underline several important aspects: the critical frequency, the double panel resonance, and the existence of an incidence angle where sound was greatly transmitted. Modal behavior of plates was introduced by Vogel.[4] Later, coupling between a panel and a cavity has been studied[5–7] and sound transmission through nonresonant modes below critical frequency has been shown. Finally, several expressions of transmission loss through single and double panels were formulated by different authors like Beranek[8] or Fahy.[9] Their models, summed up and compared with experiment in Ref. 10, are based on the mass law with additional terms enabling to take into account some particular effects like critical frequency effect or reverberant field excitation. However, for more complicated systems, other tools are necessary like finite element models. A review of numerical solutions for low frequency structural acoustic problems and their limitations was done by Atalla and Bernhard.[11] Expansion of solution on a functional base to describe structural acoustic problems was presented in Refs. 12 and 13. At high frequency statistical energy analysis was used (Refs. 14 and 15). The different methods were then applied to design simple or double panels with optimized sound insulation properties on a given frequency band. Kropp and Rebillard[16] have for example studied the case of double panels with a transfer matrix method that is not very time consuming and give accurate results compared to the experiment. It is adapted to a description of diffuse field by uncorrelated plane waves summation. Unfortunately, it is not adapted to evaluate the influence of excitation conditions such as source room geometry, source location, and panel location on transmission loss of a panel.

Transmission loss of more sophisticated panels were also studied. Guyader[17–19] studied, for example, the case of orthotropic multilayered plates, and Nilsson[20] studied the case of sandwich structures with honeycomb and foam cores. Finally, developments of numerical poroelastic models (Refs. 21 and 22) enabled to study sound transmission through finite multilayered systems containing poroelastic materials.[23]

Practically, two main difficulties appear when dealing with calculation of transmission loss of double panels. The first is related to the excitation by diffuse field. The standard approach consist in decomposing the sound field in uncorrelated plane waves as in diffuse theory and cumulating the transmission loss calculated for each angle of incidence. This method has an extremely high computation cost that can be reduced drastically using the approach proposed by Spronck[24] and Guyader[18] using radiation impedance of plate modes in a reciprocal way. Another possibility of avoiding angle summation was proposed by Coyette,[25] based on a coherence length in diffuse field. A second difficulty with waves summation is the approximation of reality by diffuse field that can be bad especially at low frequency. A better comparison with the experiment was obtained by limiting the angle of incidence in order to suppress grazing waves excitation. In addition to the difficulty of fixing a limit angle, the numerical cost of cumulating results for different incident angles remains because the approach in Refs. 18 and 24 cannot be used in this case. The method presented in this paper avoids that difficulty, calculating the cavity boundary pressure field over the blocked panel, transmission loss is calculated without angle summation, and takes into account source room characteristics. A second difficulty associated with classical methods is the global modelization of the problem that necessitates a complete calculation when one element is modified. The use of a mobility technique permits us to characterize each component of the vibroacoustic problem separately, then to calculate the transmission loss solving the interaction equation. If one element is modified, only its own characterization has to be calculated before solving interaction equations. The mobility technique introduced in Refs. 26 and 27 is now widely used in structural coupling,[28–30] and an extension to energy mobility was presented by Orefice *et al.*[31] The mobility approach for vibroa-

[a]Electronic mail: jdchazot@lva.insa-lyon.fr

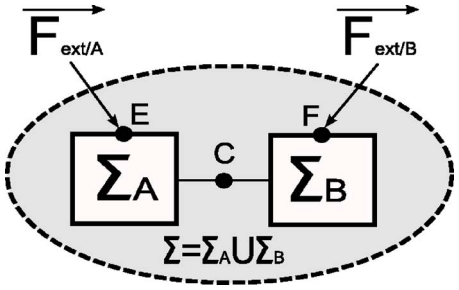

FIG. 1. Simple case of one coupling point.

coustic problems used here appears as an integral equation discretized by collocation leading to patch mobilities. This method was used previously by Ouisse *et al.*[32] for coupling acoustic subdomains.

II. PATCH-MOBILITY METHOD

A. Simple case of one coupling point

The mobility method enables us to calculate the response of vibrating coupled linear systems thanks to the knowledge of their isolated behaviors. The following example describes the principles of the mobility method. Let us consider a linear system Σ constituted of two subsystems Σ_A and Σ_B coupled at a point C (Fig. 1).

In all the following calculations, harmonic motions of angular frequency ω are assumed, and for sake of simplicity, time dependence $e^{j\omega t}$ is omitted. In a first step, transfer mobilities between two points M and Q are determined. This mobility being defined as the ratio of velocity at point M and force applied at point Q: $Y(M,Q)=V(M)/F(Q)$. From mobility $Y(M,Q)$, velocity at point M created by a force located at point Q can be calculated. However, excitation of a subsystem is produced by external forces, but also by coupling to other subsystems. This gives for subsystem A:

$$V_A(M) = \underbrace{Y_A(M,E)F_{\text{ext}\to A}(E)}_{\tilde{V}_A(M)} + \underbrace{Y_A(M,C)F_{B\to A}(C)}_{V_A^c(M)} \quad \forall M \in A. \tag{1}$$

Two velocities can be identified from Eq. (1): the velocity before coupling $\tilde{V}_A(M)$, and the velocity generated by the coupling $V_A^c(M)$. The second one is produced by the coupling force which is unknown, and appears as well in the subsystem B [notice that: $F_{B\to A}(C)=-F_{A\to B}(C)$]:

$$V_B(M) = Y_B(M,F)F_{\text{ext}\to B}(F) + Y_B(M,C)F_{A\to B}(C) \quad \forall M \in B. \tag{2}$$

To be able to find out the velocity at any point belonging to system A or B, the coupling force has to be determined. This is done with continuity condition at coupling point C: velocities of each subsystem have to be equal at the coupling point $[V_A(C)=V_B(C)]$. From these relations one can obtain the coupling force

$$F_{B\to A} = \frac{Y_B(C,F)F_{\text{ext}\to B}(F) - Y_A(C,E)F_{\text{ext}\to A}(E)}{[Y_A(C,C)+Y_B(C,C)]}. \tag{3}$$

Finally, the velocity of any point M can be calculated by using Eqs. (1) and (2).

B. Case of surface coupling with a patch-mobility method

When the coupling between subsystems is applied through a surface, Eqs. (1) and (2) must be adapted. External forces are considered surfacic as well. Tangential velocities and forces are not taken into account, that is realistic for acoustic subsystems and vibroacoustic coupling. Therefore the mobility $Y(M,Q)$ is only associated to transverse motion, and normal velocities and forces are defined as algebric values. Coupling velocities are then calculated by integrating the product of mobility and coupling (respectively, external) surfacic force over coupling (respectively, excited) surface

$$V_A(M) = \int_{S_A} [Y_A(M,E)F_{\text{ext}\to A}(E)]dS + \int_{S_c} [Y_A(M,C)F_{B\to A}(C)]dS \quad \forall M \in (A), \tag{4}$$

$$V_B(M) = \int_{S_B} [Y_B(M,F)F_{\text{ext}\to B}(F)]dS + \int_{S_c} [Y_B(M,C)F_{A\to B}(C)]dS \quad \forall M \in (B). \tag{5}$$

External forces of subsystem A (respectively, B) are applied on surface S_A (respectively, S_B), and coupling forces are applied on coupling surface S_c.

A collocation method can be used to solve the problem, separating surfaces such as $S_A=\cup_{i=1}^{N_A}S_{Ai}$ and $S_{Ai}\cap_{i\neq j}S_{Aj}=\emptyset$, $S_B=\cup_{i=1}^{N_B}S_{Bi}$ and $S_{Bi}\cap_{i\neq j}S_{Bj}=\emptyset$, $S_c=\cup_{i=1}^{N_c}S_{ci}$ and $S_{ci}\cap_{i\neq j}S_{cj}=\emptyset$. Let us first calculate averaged velocities on patch i:

$$\langle V_A\rangle_i = \int_{S_{Ai}} \sum_{j=1}^{N_A} \left\{ \int_{S_{Aj}} [Y_A(M,E)F_{\text{ext}\to A}(E)]dE \right\} dM + \int_{S_{Ai}} \sum_{j=1}^{N_c} \left\{ \int_{S_{cj}} [Y_A(M,C)F_{B\to A}(C)]dC \right\} dM \quad \forall M \in A, \tag{6}$$

$$\langle V_B\rangle_i = \int_{S_{Bi}} \sum_{j=1}^{N_B} \left\{ \int_{S_{Bj}} [Y_B(M,E)F_{\text{ext}\to B}(E)]dE \right\} dM + \int_{S_{Bi}} \sum_{j=1}^{N_c} \left\{ \int_{S_{cj}} [Y_B(M,C)F_{A\to B}(C)]dC \right\} dM \quad \forall M \in B. \tag{7}$$

Assuming in a second step that surfacic forces are constant on patches $[F(x,y)=\langle F\rangle_j$ if $(x,y)\in S_j]$, Eqs. (6) and (7) give

$$\langle V_A\rangle_i = \sum_{j=1}^{N_A} \langle\langle Y_A\rangle_i\rangle_j \langle F_{\text{ext}\to A}\rangle_j + \sum_{j=1}^{N_c} \langle\langle Y_A\rangle_i\rangle_j \langle F_{B\to A}\rangle_j, \tag{8}$$

$$\langle V_B\rangle_i = \sum_{j=1}^{N_B} \langle\langle Y_B\rangle_i\rangle_j \langle F_{\text{ext}\to B}\rangle_j + \sum_{j=1}^{N_c} \langle\langle Y_B\rangle_i\rangle_j \langle F_{A\to B}\rangle_j. \quad (9)$$

A new transfer mobility expression appears, it is the ratio of averaged patch i velocity to averaged patch j surfacic force

$$\langle\langle Y_A\rangle_i\rangle_j = \frac{\langle V\rangle_i}{\langle F\rangle_j}, \quad (10)$$

where

$$\langle V\rangle_i = \frac{\int_{S_i} V(x,y)dxdy}{S_i} \quad \text{and} \quad \langle F\rangle_j = \frac{\int_{S_j} F(x,y)dxdy}{S_j}. \quad (11)$$

Of course, assuming a constant surfacic force on each patch is an approximation, only valid if patch areas have small dimensions compared to wavelengths.

Then, velocity continuity over coupling patches gives N_c equations (one for each coupling patch)

$$\forall k \in [1,N_c] \quad \langle V_A\rangle_k = \langle V_B\rangle_k. \quad (12)$$

Hence, Eqs. (8) and (9) give $\forall k \in [1,N_c]$:

$$\sum_{j=1}^{N_c} \langle\langle Y_A\rangle_k\rangle_j \langle F_{B\to A}\rangle_j + \sum_{j=1}^{N_c} \langle\langle Y_B\rangle_k\rangle_j \langle F_{B\to A}\rangle_j = \sum_{j=1}^{N_B} \langle\langle Y_B\rangle_k\rangle_j \langle F_{\text{ext}\to B}\rangle_j - \sum_{j=1}^{N_A} \langle\langle Y_A\rangle_k\rangle_j \langle F_{\text{ext}\to A}\rangle_j. \quad (13)$$

The following matrices $[Y_A]$ and $[Y_B]$ are defined such as $Y_A(i,j)=\langle\langle Y_A\rangle_i\rangle_j$ and $Y_B(i,j)=\langle\langle Y_B\rangle_i\rangle_j$. Vectors $\{F_{B\to A}\}$, $\{F_{\text{ext}\to A}\}$, and $\{F_{\text{ext}\to B}\}$ are also defined such as $F_{B\to A}(j)=\langle F_{B\to A}\rangle_j$, $F_{\text{ext}\to A}(j)=\langle F_{\text{ext}\to A}\rangle_j$, and $F_{\text{ext}\to B}(j)=\langle F_{\text{ext}\to B}\rangle_j$.

Equation (13) can then be written in a matrix form, leading to the determination of coupling patch surfacic forces

$$\{F_{B\to A}\} = ([Y_A]+[Y_B])^{-1}([Y_B]\{F_{\text{ext}\to B}\} - [Y_A]\{F_{\text{ext}\to A}\}). \quad (14)$$

This extension of the mobility method, for surface coupling, is named the patch-mobility method and is applied in the following to sound transmission through double panels.

III. VIBROACOUSTIC RESPONSE OF A DOUBLE PANEL CALCULATED BY THE PATCH-MOBILITY METHOD

In this section, the patch-mobility method is applied to the vibroacoustic response of a double panel coupled to a cavity and radiating in the open external space.

In a first step, the system is divided into subsystems (cf. Fig. 2): A: emission chamber, B: first panel, C: cavity between the two panels, D: second panel, and E: semi-infinite medium.

Coupling surfaces are defined as: S_{AB} (respectively, S_{BC}, S_{CD}, S_{DE}) is the coupling surface between subsystems A and B (respectively B and C, C and D, D and E).

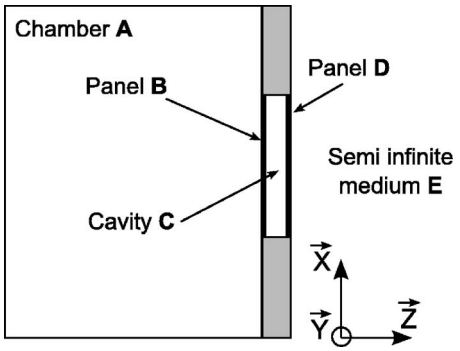

FIG. 2. Sketch of double panel coupled with a source room and a semi-infinite medium.

Equations governing patch velocities of plates, room, cavity, and infinite acoustic medium, write:

For the source room coupling surface

$$\langle V_A\rangle_i = \langle \tilde{V}_A\rangle_i + \sum_{j=1}^{N_{AB}} \langle\langle Y_A\rangle_i\rangle_j \langle F_{(B\to A)}\rangle_j. \quad (15)$$

For the first panel

$$\langle V_B\rangle_i = \langle \tilde{V}_B\rangle_i + \sum_{j=1}^{N_{AB}} \langle\langle Y_B\rangle_i\rangle_j \langle F_{(A\to B)}\rangle_j + \sum_{j=1}^{N_{BC}} \langle\langle Y_B\rangle_i\rangle_j \langle F_{(C\to B)}\rangle_j. \quad (16)$$

For the cavity coupling surfaces

$$\forall i \in S_{BC}: \langle V_{C1}\rangle_i = \langle \tilde{V}_{C1}\rangle_i + \sum_{j=1}^{N_{BC}} \langle\langle Y_{C1}\rangle_i\rangle_j \langle F_{(B\to C)}\rangle_j + \sum_{k=1}^{N_{CD}} \langle\langle Y_{C1}\rangle_i\rangle_k \langle F_{(D\to C)}\rangle_k, \quad (17)$$

$$\forall i \in S_{CD}: \langle V_{C2}\rangle_i = \langle \tilde{V}_{C2}\rangle_i + \sum_{j=1}^{N_{CD}} \langle\langle Y_{C2}\rangle_i\rangle_k \langle F_{(D\to C)}\rangle_k + \sum_{k=1}^{N_{BC}} \langle\langle Y_{C2}\rangle_i\rangle_j \langle F_{(B\to C)}\rangle_j. \quad (18)$$

For the second panel

$$\langle V_D\rangle_i = \langle \tilde{V}_D\rangle_i + \sum_{k=1}^{N_{CD}} \langle\langle Y_D\rangle_i\rangle_k \langle F_{(C\to D)}\rangle_k + \sum_{k=1}^{N_{DE}} \langle\langle Y_D\rangle_i\rangle_k \langle F_{(E\to D)}\rangle_k. \quad (19)$$

For the semi-infinite medium coupling surface

$$\langle V_E\rangle_i = \langle \tilde{V}_E\rangle_i + \sum_{k=1}^{N_{DE}} \langle\langle Y_E\rangle_i\rangle_k \langle F_{(D\to E)}\rangle_k. \quad (20)$$

The complete set of equations [Eqs. (15)–(20)] describe all the physical interactions taking part in the vibroacoustic response of the double panel. Nevertheless, some of these

phenomena can be neglected. For example, the first panel excitation can be separated in two acoustic fields: acoustic room response with blocked panel and pressure radiated by the panel. The radiated field, coming from the plate induced vibrations, is usually neglected as a second order phenomenon. On the contrary, the coupling between the cavity C and the two panels B and D is much more important. The small volume of the cavity C produces a high cavity stiffness that has a real effect upon the vibrations of the double panel.

After the discussed simplifications, Eqs. (16)–(19) write:

First panel

$$\langle V_B\rangle_i = \langle \tilde{V}_B\rangle_i + \sum_{j=1}^{N_{BC}} \langle\langle Y_B\rangle_i\rangle_j \langle F_{(C\to B)}\rangle_j. \tag{21}$$

Cavity

$$\forall i \in S_{BC}: \langle V_{C1}\rangle_i = \sum_{j=1}^{N_{BC}} \langle\langle Y_{C1}\rangle_i\rangle_j \langle F_{(B\to C)}\rangle_j + \sum_{k=1}^{N_{CD}} \langle\langle Y_{C1}\rangle_i\rangle_k \langle F_{(D\to C)}\rangle_k, \tag{22}$$

$$\forall i \in S_{CD}: \langle V_{C2}\rangle_i = \sum_{k=1}^{N_{CD}} \langle\langle Y_{C2}\rangle_i\rangle_k \langle F_{(D\to C)}\rangle_k + \sum_{j=1}^{N_{BC}} \langle\langle Y_{C2}\rangle_i\rangle_j \langle F_{(B\to C)}\rangle_j. \tag{23}$$

Second panel

$$\langle V_D\rangle_i = \sum_{k=1}^{N_{CD}} \langle\langle Y_D\rangle_i\rangle_k \langle F_{(C\to D)}\rangle_k. \tag{24}$$

Excitation appears in Eq. (21) as a patch velocity vector before coupling $\langle \tilde{V}_B\rangle_i$. It is calculated using blocked patch pressures (P_{Blocked}) applied to the first panel by the acoustic field in the source room. The first panel velocity before coupling is then calculated as follows:

$$\langle \tilde{V}_B\rangle_i = \sum_j \langle\langle Y_B\rangle_i\rangle_j \langle P\rangle_{j(\text{Blocked})} S_j. \tag{25}$$

Blocked patch pressures are calculated by integrating the pressure generated by a source in the emission chamber over the panel assumed to be rigid (blocked). Therefore room dimensions, excitation location, and position of the aperture in the room wall are, hence, taken into account. For rectangular cavity, modes are well known and calculation of room response is straightforward. Of course for large room the computation can be time consuming. However, for a given room configuration, blocked patch pressures are only calculated once whatever the plates under study.

Finally, continuity conditions over coupling surfaces S_{BC} and S_{CD} are written: $\forall i \in S_{BC}$: $\langle V_B\rangle_i = \langle V_C\rangle_i$, and $\forall i \in S_{CD}$: $\langle V_C\rangle_i = \langle V_D\rangle_i$. It yields to

$$\begin{Bmatrix} \langle \tilde{V}_1\rangle_i \\ 0 \end{Bmatrix} = \begin{bmatrix} \langle\langle Y_{C1}\rangle_i\rangle_j + \langle\langle Y_B\rangle_i\rangle_j & \langle\langle Y_{C1}\rangle_i\rangle_k \\ \langle\langle Y_{C2}\rangle_i\rangle_j & \langle\langle Y_{C2}\rangle_i\rangle_k + \langle\langle Y_D\rangle_i\rangle_k \end{bmatrix} \times \begin{Bmatrix} \langle F_{(B\to C)}\rangle_j \\ \langle F_{(D\to C)}\rangle_k \end{Bmatrix}. \tag{26}$$

Solving the linear system (26) allows us to get coupling forces $\langle F_{(B\to C)}\rangle_j$ and $\langle F_{(D\to C)}\rangle_k$ and then to calculate patch velocities after coupling by using Eqs. (21)–(24).

IV. PANEL PATCH MOBILITIES

In this section, panel mobilities are derived thanks to the Love–Kirchhoff equation of motion (flexural vibration of thin plates)

$$-\omega^2 \rho h U(x,y) + D^* \nabla^4 [U(x,y)] = P(x,y), \tag{27}$$

where $D^* = E^* h^3 / 12(1-\nu^2)$, and E^* is the complex Young modulus which takes into account structural damping such as $E^* = E(1+j\eta_s)$, and η_s is the damping loss factor.

The excitation term is defined on patch j as follows:

$$P(x,y) = \begin{cases} \dfrac{\langle F\rangle_j}{S_j} & \text{if } (x,y) \in \text{patch } j \\ 0 & \text{else} \end{cases}.$$

The modal expansion of the plate transverse displacement with simply supported boundary conditions writes

$$U(x_M, y_M) = \sum_{pq} a_{pq} \Phi_{pq}(x_M, y_M), \tag{28}$$

where mode shapes are given by

$$\Phi_{pq}(x,y) = \sin\left(\frac{p\pi}{L_x}x\right)\sin\left(\frac{q\pi}{L_y}y\right). \tag{29}$$

Incorporating Eq. (28) into Eq. (27), and using modes orthogonality yield to the modal amplitude

$$a_{pq} = \frac{\langle F\rangle_j \left[\int_j \Phi_{pq}(x,y)dS\right]}{S_j (K^*_{pq} - \omega^2 M_{pq})} \tag{30}$$

where $K^*_{pq} = \int_S D^* \Phi_{pq} \nabla^4(\Phi_{pq}) dS$, $M_{pq} = \int_S \rho h \Phi^2_{pq} dS$, and $\omega^*_{pq} = \sqrt{K^*_{pq}/M_{pq}}$.

The patch mobility as defined by Eq. (10) is then obtained

$$\langle\langle YP\rangle_i\rangle_j = \frac{j\omega}{S_i S_j} \sum_{pq} \frac{\left[\int_i \Phi_{pq}(x,y)dS\right]\left[\int_j \Phi_{pq}(x,y)dS\right]}{M_{pq}[\omega^*_{pq} - \omega^2]}. \tag{31}$$

Figure 3 shows an example of input and transfer panel patch mobilities versus frequency calculated for an aluminum panel (Lx=1.5 m, Ly=0.96 m, Lz=0.002 m). As expected, transfer patch-mobility magnitude (thin curve) is lower than input patch-mobility magnitude (thick curve). It can also be noticed that as frequency increases, mobility curve is smoothed, due to modal overlap. However, this is more marked on input patch mobility than on transfer patch mobility.

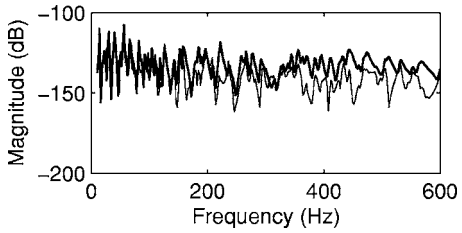

FIG. 3. Panel patch mobility—Thick line: Input patch mobility (patch 42), Thin line: Transfer patch mobility (patch 42/72)—Aluminium panel: $Lx=1.5$ m, $Ly=0.96$ m, $Lz=0.002$ m—Patch size: $\Delta x=7.9$ cm, $\Delta y=7.4$ cm—Patch 42: $X=[0.24\text{ m};\ 0.32\text{ m}]$, $Y=[0.15\text{ m};\ 0.22\text{ m}]$—Patch 72: $X=[1.11\text{ m};\ 1.18\text{ m}]$, $Y=[0.22\text{ m};\ 0.30\text{ m}]$.

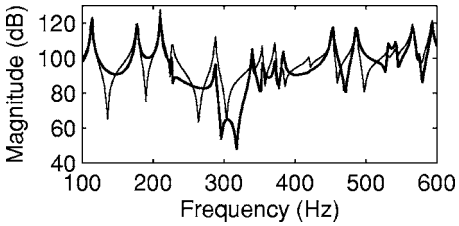

FIG. 4. Acoustic patch impedance—Thin line: Input patch impedance (patch 42), Thick line: Transfer patch impedance (patch 42/72)—Cavity: $Lx=1.5$ m, $Ly=0.96$ m, $Lz=0.01$ m—Patch size: $\Delta x=7.9$ cm, $\Delta y=7.4$ cm—Patch 42: $X=[0.24\text{ m};\ 0.32\text{ m}]$, $Y=[0.15\text{ m};\ 0.22\text{ m}]$—Patch 72: $X=[1.11\text{ m};\ 1.18\text{ m}]$, $Y=[0.22\text{ m};\ 0.30\text{ m}]$.

V. ACOUSTIC PATCH MOBILITIES OF A CAVITY

A. Problem description

Neumann inhomogeneous problem (32) is considered, that is to say an acoustic cavity with rigid wall boundary condition on $\partial\Omega_-$ and excited by a boundary velocity field on $\partial\Omega_+$. The aim is to find the pressure at any point M, radiated by a vibrating surface of normal velocity V_n:

$$\Delta P(M)+k^2P(M)=0 \quad \forall M\in\Omega,$$

$$\frac{\partial P(Q)}{\partial n}=-j\rho\omega V_n(Q) \quad \forall Q\in\partial\Omega_+,$$

$$\frac{\partial P(Q)}{\partial n}=0 \quad \forall Q\in\partial\Omega_-. \tag{32}$$

Acoustic damping is introduced with a complex wave number: $k^*=\omega/c^*=\omega/[c\sqrt{(1+j\eta_a)}]$, and to solve this problem, expansion on modes of undamped cavity is used.

B. Pressure modal expansion

Modal expansion is used to describe the cavity pressure field

$$P(M)=\sum_p a_p\psi_p(M). \tag{33}$$

After some calculations (cf. Appendix A), pressure radiated at point M is given by

$$P(M)=\sum_p\left(\frac{\int_{\partial\Omega_+}\{\psi_p(Q)[-j\rho\omega V_n(Q)]\}dQ}{(k^{*2}-k_p^2)N_p}\psi_p(M)\right). \tag{34}$$

To obtain the acoustic transfer impedance between two patches i and j, a uniform normal velocity V_n is given on patch j, and pressure (34) is integrated over the observation patch i:

$$\langle\langle Z\rangle_i\rangle_j=\frac{\int_{S_i}P(M)\bar{n}_i dS_i}{\underline{\int_{S_i}\bar{V}_n(M)dS_j}}=\frac{\int_{S_i}P(M)\bar{n}_i dS_i}{\langle V_n\rangle_j}=\frac{\langle F\rangle_i}{\langle V_n\rangle_j}.$$
$$S_j$$

With pressure modal expansion, the following expression for patch acoustic impedance is obtained:

$$\langle\langle Z\rangle_i\rangle_j=-j\rho\omega\sum_p\frac{[\int_{Si}\psi_p(x,y)dS][\int_{Sj}\psi_p(x,y)dS]}{(k^{*2}-k_p^2)N_p}. \tag{35}$$

Equation (35) is the general cavity acoustic impedance expression. For a rectangular cavity with rigid walls, analytical expression of mode shapes can be derived

$$\psi_{pqr}(M)=\cos\left(\frac{p\pi x}{Lx}\right)\cos\left(\frac{q\pi y}{Ly}\right)\cos\left(\frac{r\pi z}{Lz}\right). \tag{36}$$

A mode being defined with three indices, expression (35) writes

$$\langle\langle Z\rangle_i\rangle_j=-j\rho\omega \times\sum_{pqr}\frac{[\int_{Si}\psi_{pqr}(x,y,Z_i)dxdy][\int_{Sj}\psi_{pqr}(x,y,Z_j)dxdy]}{(k^{*2}-k_{pqr}^2)N_{pqr}}. \tag{37}$$

The global impedance matrix describing the cavity behavior writes

$$\begin{pmatrix}\langle F\rangle_1\\ \vdots\\ \langle F\rangle_n\end{pmatrix}=\underbrace{\begin{bmatrix}\langle\langle Z\rangle_1\rangle_1 & \cdots & \langle\langle Z\rangle_1\rangle_n\\ \vdots & \ddots & \vdots\\ \langle\langle Z\rangle_n\rangle_1 & \cdots & \langle\langle Z\rangle_n\rangle_n\end{bmatrix}}_{[Z]}\cdot\begin{pmatrix}\langle V\rangle_1\\ \vdots\\ \langle V\rangle_n\end{pmatrix}$$

Then patch mobility matrix is obtained as the inverse of patch impedance matrix

$$\begin{pmatrix}\langle V\rangle_1\\ \vdots\\ \langle V\rangle_n\end{pmatrix}=\underbrace{\begin{bmatrix}\langle\langle Y\rangle_1\rangle_1 & \cdots & \langle\langle Y\rangle_1\rangle_n\\ \vdots & \ddots & \vdots\\ \langle\langle Y\rangle_n\rangle_1 & \cdots & \langle\langle Y\rangle_n\rangle_n\end{bmatrix}}_{[Y]=[Z]^{-1}}\cdot\begin{pmatrix}\langle F\rangle_1\\ \vdots\\ \langle F\rangle_n\end{pmatrix}.$$

Figure 4 presents two acoustic patch input impedances versus frequency of a cavity ($Lx=1.5$ m, $Ly=0.96$ m, $Lz=0.01$ m) that show its modal behavior. One can see also that modes are responding differently according to patch location. Acoustic patch impedances between patches located on opposite boundary surfaces such as $Z_i\neq Z_j$ are not presented since they are not different from impedances between patches located on the same boundary surface such as $Z_i=Z_j$. This is of course due to the small thickness of the cavity, and the studied frequency range.

Figure 5 presents two acoustic patch mobilities versus frequency for the same cavity ($Lx=1.5$ m, $Ly=0.96$ m, Lz

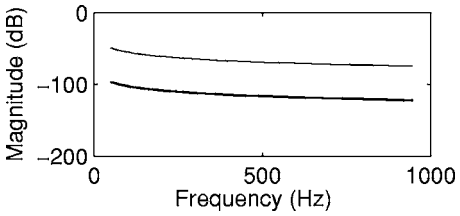

FIG. 5. Acoustic patch mobility—Thin line: Input patch mobility (patch 42), Thick line: Transfer patch mobility (patch 42/72)—Cavity: Lx=1.5 m, Ly=0.96 m, Lz=0.01 m—Patch size: Δx=7.9 cm, Δy=7.4 cm—Patch 42: X=[0.24 m; 0.32 m], Y=[0.15 m; 0.22 m]—Patch 72: X=[1.11 m; 1.18 m], Y=[0.22 m; 0.30 m].

=0.01 m). Results are surprising since patch mobilities do not exhibit the modal behavior that can be seen on patch impedances. To explain this strange result, one has to remember that direct patch mobility calculation will be obtained by solving the Dirichlet problem (null boundary pressure except on excited patch), and calculating the patch averaged velocity created at boundary. Cavity resonances with Dirichlet boundary conditions are obviously different from that of a cavity with Neumann boundary conditions. The first resonance of the rectangular cavity with Dirichlet boundary conditions is equal to $(c/2\pi)\sqrt{(\pi/Lx)^2+(\pi/Ly)^2+(\pi/Lz)^2}$, that is to say 17 000 Hz. That explains why no resonance appears in the studied frequency band.

VI. SEMI-INFINITE MEDIUM

This section describes the method used to calculate the power radiated into the semi-infinite receiving medium.

A. Radiated pressure

Radiation impedance is defined as the ratio of averaged patch i radiated pressure to averaged patch j velocity: $\langle\langle Z\rangle_i\rangle_j=\langle P_{\text{rad}}\rangle_i/\langle V\rangle_j$. The radiated pressure can thus be calculated from panel patch velocities (cf. Fig. 6).

Radiation impedance calculations are based on Rayleigh's integral and are detailed in Appendix B. A particular case is defined when emitting and receiving patch are the same (i.e., $i=j$). In this case radiation impedance expression is given by Eq. (38) where "a_i" is the radius of a circular patch of surface S_i. Otherwise, when emitting and receiving patch are different (i.e., $i\neq j$) Eq. (39) is used to calculate radiation impedance where d_{ij} is the distance between two patches central points

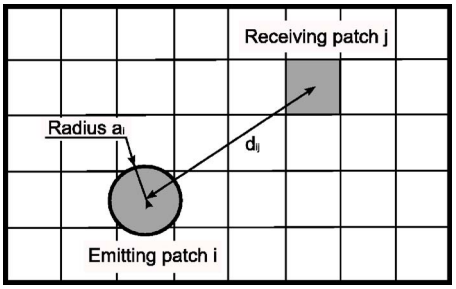

FIG. 6. Radiating panel description.

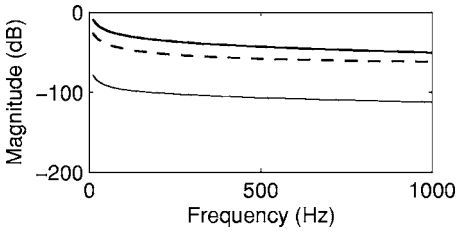

FIG. 7. Patch radiating mobility—Thick solid line: Input patch mobility, Thick dotted line: Transfer patch mobility with d_{ij}=0.08 m, Thin line: Transfer patch mobility with d_{ij}=0.84 m—Panel: Lx=0.96 m, Lz=1.5 m–Patch size: Δx=7.9 cm, Δy=7.4 cm.

$$\langle\langle Z\rangle_i\rangle_i=\frac{\langle P_{\text{rad}}\rangle_i}{\langle V\rangle_i}=\rho_0 c[1-\exp^{-jka}], \tag{38}$$

$$\langle\langle Z\rangle_i\rangle_j=\frac{\langle P_{\text{rad}}\rangle_i}{\langle V\rangle_j}=\frac{1}{2\pi}\rho_0 j\frac{\exp^{-jkd_{ij}}}{d_{ij}}S_j. \tag{39}$$

Radiation patch mobilities are obtained by inversion of impedance matrix calculated from previous Eqs. (38) and (39). Figure 7 illustrates radiation patch mobility behavior. As one can see, radiation patch mobility magnitude decreases with frequency and also when distance between radiating and receiving patch d_{ij} decreases.

B. Radiated power

Radiated power is calculated from patch velocities and radiated patch pressures, and can be written using radiation patch mobilities (40):

$$I_{\text{rad}}=\frac{1}{2}\sum_i \text{Re}\{\langle V\rangle_i^*\langle P_{\text{rad}}\rangle_i\}=\frac{1}{2}([Y_{\text{rad}}]^{-1}\{V\})'\{V\}^*. \tag{40}$$

VII. SOURCE ROOM MODELING

This section describes a simple way to model the source room as depicted in Fig. 8 using its modal behavior. Two quantities are presented: the mean quadratic room pressure that is used to calculate double panel transmission loss, and blocked patch pressures (BPP) that are used to calculate patch velocities before coupling in Eq. (25). To calculate these quantities one has to replace the flexible panel by a rigid wall.

Standard room response modal expansion writes

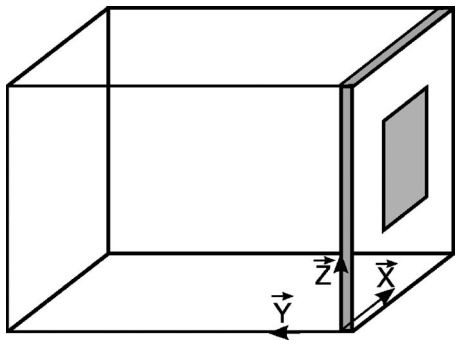

FIG. 8. Sketch of the excitation room.

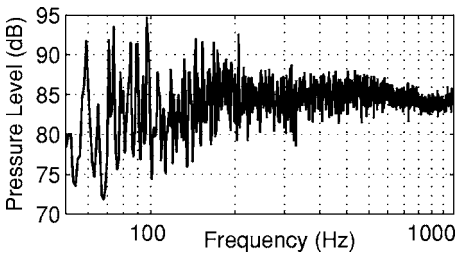

FIG. 9. Room pressure level—room dimensions: $lx=11.5$ m, $ly=8.69$ m, $lz=4.03$ m—Source at: $Xs=2$ m, $Ys=4$ m, $Zs=1$ m, amplitude: $S_0=2$—Cutoff frequency: 187 Hz.

$$P(x,y,z)=\sum_{p,q,r} A_{pqr}\psi_{pqr}(x,y,z), \tag{41}$$

where $A_{pqr}=\int_\Omega \psi_{pqr}(x,y,z)S(x,y,z)d\Omega/(k^{*2}-k_{pqr}^2)N_{pqr}$, and $N_{pqr}=\int_\Omega \psi_{pqr}^2(x,y,z)d\Omega$. A point source excitation is used such as: $S(x,y,z)=S_0\delta(x-x_0)\delta(y-y_0)\delta(z-z_0)$. The wave number k^* takes into account fluid damping with a complex sound speed: $k^*=\omega/c^*=\omega/c\sqrt{(1+j\eta_r)}$, where $\eta_r=2.2/fT_r$ and T_r is reverberation time.

The source room, being assumed to be a parallelepipedic-shaped room with rigid walls, has the following mode shapes:

$$\psi_{pqr}(x,y,z)=\cos\left(\frac{p\pi}{lx}x\right)\cos\left(\frac{q\pi}{ly}y\right)\cos\left(\frac{r\pi}{lz}z\right).$$

A. Quadratic room pressure

Mean quadratic room pressure calculation that is useful in the prediction of the transmission loss, is straightforward

$$P_r^2=\sum_{pqr}\frac{|A_{pqr}^2|\varepsilon_p\varepsilon_q\varepsilon_r}{8}$$

$$\text{and } \varepsilon_p=\begin{cases}1 & \text{if } p=0\\ 2 & \text{if } p\neq 0\end{cases}. \tag{42}$$

Figure 9 shows the mean quadratic pressure given by Eq. (42). At low frequency, despite the large room volume ($\approx$400 m^3), modal behavior is predominant. Modes (2,1,1) at 55 Hz, (1,2,1) at 59 Hz, (2,2,1) at 65 Hz are clearly identified. On the contrary, at higher frequency modal overlap occurs, reducing the mean quadratic room pressure variations with frequency. The cut off frequency given by $f_c=\sqrt{c^3T_r/8.8\pi V}$ corresponds roughly to the limit between modal and diffuse field behavior. Above that frequency, modal separation is lower than the −3 dB bandwidth. In the present case ($T_r\approx 10$ s and $V\approx 400$ m^3), the cutoff frequency is equal to 187 Hz.

B. Blocked patch pressure

Modal expansion (41) of the room response gives the pressure distribution in the room. Blocked patch pressures over a panel are then calculated by integrating the room pressure over a patch surface located on a rigid wall

$$\langle P\rangle_i=\int_{S_i}\left[\sum_{p,q,r} A_{pqr}\psi_{pqr}(x,y_0,z)\right]dxdz. \tag{43}$$

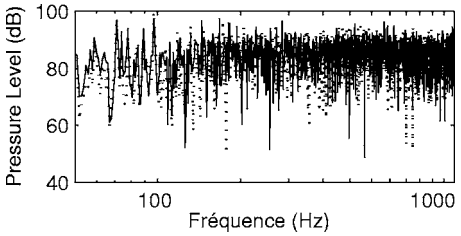

FIG. 10. Blocked patch pressure level on two patches—Dotted line: patch 124, Solid line: patch 1—Located at $X_{124}=6$ m, $Y_{124}=0$ m, $Z_{124}=1.75$ m, and $X_1=5.245$ m, $Y_1=0$ m, $Z_1=1.27$ m—Room dimensions: $lx=11.5$ m, $ly=8.69$ m, $lz=4.03$ m—Patch size: $\Delta X=0.08$ m, $\Delta Z=0.074$ m—Source position: $Xs=2$ m, $Ys=4$ m, $Zs=1$ m, amplitude: $S_0=2$—cutoff frequency: 187 Hz.

These blocked patch pressures are used in Eq. (25) to calculate panel patch velocities before coupling and enable to solve the set of Eqs. (21)–(24).

Figure 10 illustrates variations with frequency of two blocked patch pressures. Peaks and antipeaks can have different values, but both curves have the same averaged value over frequency (85 dB). These differences come obviously from mode shapes. Moreover, a large amplitude of variation with frequency is noticed even at high frequency, contrary to space averaged pressure in the room presented in Fig. 9. Blocked patch pressure behavior is a bit surprising compared to standard way of thinking on reverberant pressure in large room, however, it is a quasilocal quantity, contrary to reverberant pressure that is averaged over the room volume. Contrary to mean quadratic pressure, no obvious frequency limit between modal behavior and diffuse field, such as the cutoff frequency (187 Hz), can be observed on blocked patch pressure.

Figure 11 presents the blocked patch pressure distribution pattern at two frequencies for two window locations on source room wall. As a general rule, the blocked patch pressure patterns display clearly the acoustic wave length at each frequency. However, a change in pressure distribution is observed for the two window locations, that leads to transmission loss differences particularly at low frequency.

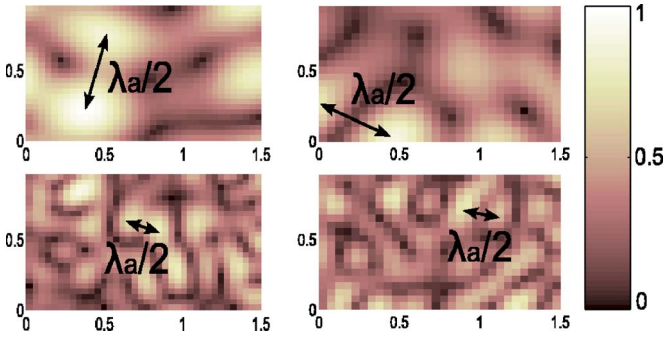

FIG. 11. (Color online) Blocked patch pressure magnitude for two window locations ($lx=0.96$ m, $lz=1.5$ m)—on the top: 400 Hz—on the bottom: 1000 Hz—on the left, the window is centered on point $X=6$ m, $Y=0$ m, $Z=1.75$ m—on the right the window is centered on point $X=6.96$ m, $Y=0$ m, $Z=2.78$ m—Room dimensions: $lx=11.5$ m, $ly=8.69$ m, $lz=4.03$ m—Patch size: $\Delta X=0.04$ m, $\Delta Z=0.037$ m—Source position: $Xs=2$ m, $Ys=4$ m, $Zs=1$ m, amplitude: $S_0=2$—cutoff frequency: 187 Hz.

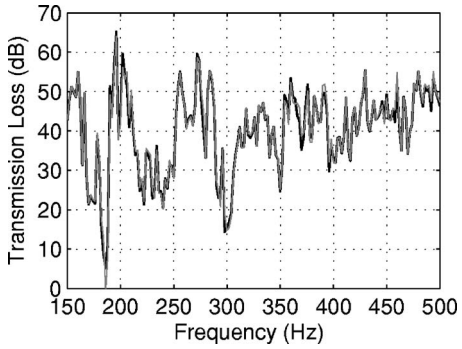

FIG. 12. Transmission loss comparison with two meshes—Thick line: mesh 30×20, Thin grey line: mesh 8×5—Double panels in steel ($Lx=0.6$ m, $Lz=0.4$ m), 2 and 1.5 mm thickness, separated by 1 cm of air.

VIII. ACOUSTIC TRANSMISSION THROUGH DOUBLE PANELS

This section presents the transmission loss calculation through a double panel.

A. Transmission loss calculation

Transmission loss τ is defined as the ratio of transmitted power Π_t to incident power Π_i. Transmitted power can be calculated thanks to the mobility method with Eq. (40). With the procedure of standard measurement of transmission loss, incident power is deduced from mean quadratic room pressure using a classical result of Sabine's theory: $\Pi_i = S(P_r^2/4\rho_0 c)$. Of course the assumption of Sabine's theory is not exactly verified for standard rectangular rooms specially at low frequency, but is nevertheless used for sake of simplicity.

This way of calculating transmission loss in a reverberant field (i.e., by using blocked patch pressures) avoids integration over incidence angles that is usually employed. When good accuracy is desired, several incidence angles must be considered with a plane wave summation method, and time needed to compute transmission loss becomes tremendous compared to time necessary with room blocked patch pressures excitation.

B. Convergence criterion

The usual mesh condition for finite element analysis is given by $\Delta L < \lambda_{\min}/6$, and sometimes $\lambda_{\min}/4$ is admitted.

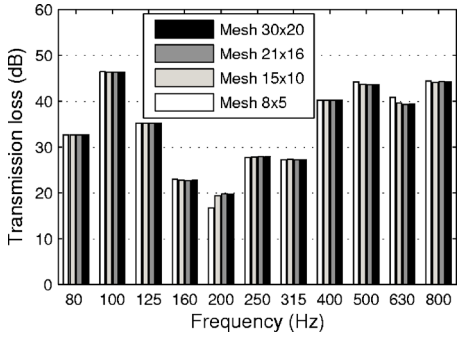

FIG. 13. Mesh comparison with third octave analysis—Double panels in steel ($Lx=0.6$ m, $Lz=0.4$ m), 2 and 1.5 mm thickness, separated by 1 cm of air.

TABLE I. Maximal frequency given by different criterions.

Criterion	$\lambda_a/6$	$\lambda_a/4$	$\lambda_a/2$	$\lambda_s/6$	$\lambda_s/4$	$\lambda_s/2$
Mesh 30×20	2833	4250	8500	1026	2309	9237
Mesh 21×16	1983	2975	5950	503	1132	4526
Mesh 15×10	1416	2125	4250	256	577	2309
Mesh 8×5	708	1062	2125	64	144	577

If we assume that the same criterion can be used for the patch mobility method, therefore the maximum patch length necessary to go up to 1000 Hz is 5.7 cm for acoustic media (8.5 cm with $\lambda_{\min}/4$). For the structure, one needs to look at the bending wave length $\lambda = c_{flx}/f = (1/f)\sqrt{\omega}\sqrt[4]{Eh^2/\rho\times12(1-\nu^2)}$.

Four meshes have been tested to find which criterion had to be taken with linear elements. Figure 12 presents the transmission loss calculated with two meshes, and Fig. 13 shows the transmission loss comparison with a third octave analysis for each mesh. Table I gives structural and acoustical criterions associated with each mesh.

Meshes 30×20, 21×16, and 15×10 give similar results: the three curves are superimposed and cannot be distinguished. The 8×5 mesh curve starts to be slightly different around 150–200 Hz. This frequency can be viewed as the limit frequency given by the $\lambda_s/4$ criterion. However, results obtained with mesh 8×5 can be accepted up to 577 Hz which is the limit given by criterion $\lambda_s/2$. This result agrees with criterions found in Ref. 33 where authors showed that a $\lambda/2$ criterion could be taken to couple linear acoustic problems with a similar method (patch transfer functions).

In the following, presented results are obtained with elementary plane rectangular patches verifying the $\lambda_s/2$ criterion.

C. Influence of room characteristics on acoustic transmission

Several studies have shown transmission loss measurements differences in interlaboratory comparisons at low frequencies not only for small reverberant rooms, but even for large ones. In this section, two large rooms of same volumes are studied (cf. Table II). Transmission loss results for both rooms are plotted in Fig. 14. Differences of transmission loss are up to 6 dB for the same double panel. At 78 Hz, it can be explained by looking at the BPP distribution (Fig. 15) that are quite different for the two source rooms. This result was expected since it is known that for frequencies below the cutoff frequency, the acoustic field cannot be considered as diffuse. At higher frequencies differences are still noticeable, that is more unexpected. As can be seen in Fig. 15, though

TABLE II. Test room dimensions, source location, and panel location.

	lx (m)	ly (m)	lz (m)	X_{source} (m)	Y_{source} (m)	Z_{source} (m)	$X_{\text{centralpatch}}$ (m)	$Z_{\text{centralpatch}}$ (m)
Room 1	4.03	5	10	0.8	2	2.5	1.75	5
Room 2	10	5	4.03	2	2	1	5	1.75

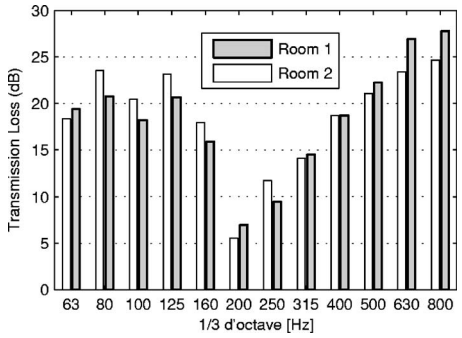

FIG. 14. Comparison between two rooms—Double panels in aluminum (Lx=0.96 m, Lz=1.5 m), 2 and 1.5 mm thickness, separated by 3 cm of air—Patch size: ΔX=0.08 m, ΔZ=0.074 m—Source amplitude: S_0=2—cutoff frequency: 187 Hz.

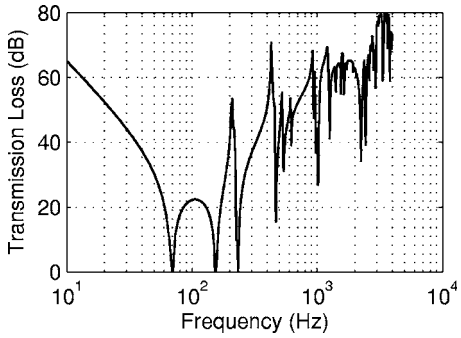

FIG. 16. Normal incidence sound transmission loss of a double aluminum panel (0.35 m by 0.22 m, 1 mm thickness) separated by 0.0762 m of air—Results obtained with the patch-mobility method.

the field is more diffuse at 800 Hz, the two rooms do not provide the same pressure distribution over the panel. Moreover, as long as structural wavelength is not much higher than acoustical wavelength, differences in pressure distribution over the panel will have an effect on the panel response and on sound transmission. Therefore, even above the cutoff frequency, panel excitation depends on room characteristics, source location, and aperture location.

IX. COMPARISON WITH A FINITE ELEMENT MODEL

The patch-mobility method has been applied to the double panel studied by Panneton and Atalla with a finite element model in Ref. 23: simply supported aluminum plates (0.35 m by 0.22 m, 1 mm thickness) separated by 0.0762 m of air. Excitation is realized by a normal incident plane wave. Results obtained with patch mobility method are presented up to 4000 Hz in Fig. 16. A good agreement is observed with results obtained by Panneton and Atalla in Ref. 23, at least up to maximal finite element calculation frequency (500 Hz).

Two particular aspects of the patch-mobility method must be underlined in this comparison: the mesh criterion in $\lambda/2$ that is very coarse compared to the criterion in $\lambda/6$ used in finite element method (FEM) and the possibility to characterize each subsystem separately with the patch mobility method contrary to FEM (if one element is modified, only its own characterization has to be calculated before solving interaction equations).

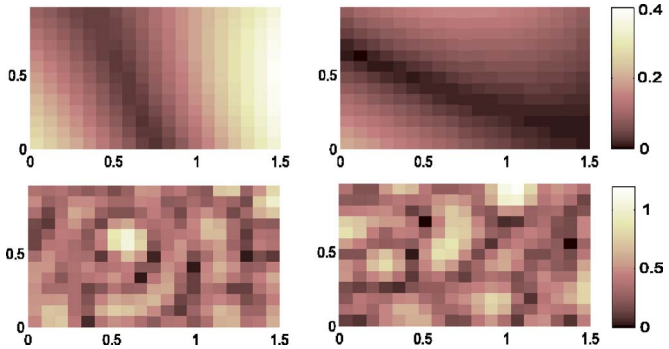

FIG. 15. (Color online) Blocked patch pressure distribution—Top: 78 Hz—Bottom: 800 Hz—Left: room 1, Right: room 2.

X. EXPERIMENTAL RESULTS

Figure 17 presents the experimental setup. Measurements of transmitted power were done using intensity technique with a 50 mm intensity probe located at 20 cm from the radiating panel. 100 points have been used to measure radiated intensity. Source room is a reverberant room (lx =11.5 m, ly=8.69 m, lz=4.03 m, cutoff frequency=187 Hz) where walls are not parallels and with diffusers in the corners. Five microphones in the reverberant chamber enabled to measure reverberant pressure. Receiving room is not reverberant and is treated to be the most isolated from exterior sound and with a high sound absorption to limit reflections of radiated sound by tested panel. It can thus be considered as a semi anechoic enclosure.

Transmission loss of a double aluminum panel was then measured. The double panel dimensions were: width 0.96 m, length 1.5 m, thickness 2 mm and 1.5 mm, air gap thickness 1 cm. Panel critical frequencies are 7961 Hz for the aluminum panel of 1.5 mm thickness, and 5971 Hz for the aluminum panel of 2 mm thickness. The theoretical mass-spring-mass frequency for diffuse field is 328 Hz.

Figures 18 and 19 show comparisons of double panels transmission loss obtained by experiment and with the patch-mobility model. The model gives the same tendency as measurements and differences observed on some third octaves are quite reasonable. Indeed, compared to reproducibility and repeatability values mentioned in norm ISO 140-3, differences observed with third octave analysis between the model and the experiment are quiet good (example of repeatability values given by the norm 4.5 dB at 100 Hz and 1.5 dB at

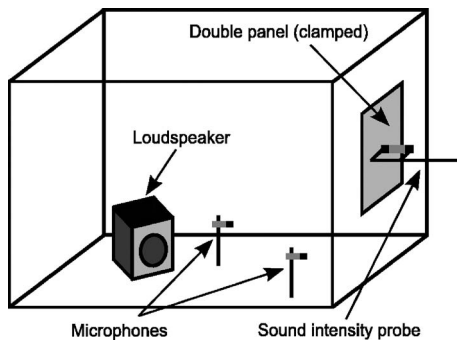

FIG. 17. Experimental setup.

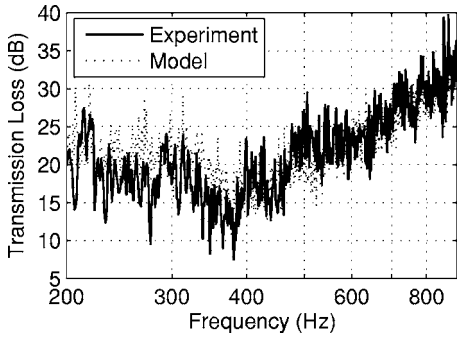

FIG. 18. Comparison with experiment—Solid line: experiment, dotted line: model—Double aluminum panel (Lx=0.96 m, Lz=1.5 m), 2 and 1.5 mm thickness, separated by 3 cm of air, centered on point X=6 m, Y=0 m, Z=1.75 m—Room dimensions: lx=11.5 m, ly=8.69 m, lz=4.03 m—Patch size: ΔX=0.08 m, ΔZ=0.074 m—Source at: Xs=2 m, Ys=4 m, Zs=1 m, amplitude: S_0=2—cutoff frequency: 187 Hz—structural damping: 0.06—fluid damping: 0.035.

1000 Hz). An intercomparison of laboratory measurements, realized in 23 European laboratories, shows also a high dispersion of airborne sound insulation measurements. This sudy is presented in Ref. 33. Dispersions are not negligible, and even at high frequencies differences up to 5 dB are observed. Therefore, the mobility model can be considered as reliable to predict transmission loss through double panels.

Concerning cavity damping, particular care is needed to determine its value. Indeed, cavity damping is known to be very influential upon sound transmission between the double panel resonance frequency and the critical frequencies of the panels. As mentioned in Ref. 34, cavity damping can be much higher than typical fluid damping due to neglected physical phenomenon like viscous and thermal dissipations near boundaries. In this reference, cavity damping is set to 10^{-3} while damping in surrounding fluid is set to 10^{-8}. In the following, cavity damping has been used to adjust the model with experiment, and a value of 0.035 has been found in the case of the double panel with a cavity of 1 cm thickness. It is also important to notice that cavity damping depends on the air layer thickness. Indeed, for thicker layers, effects of viscous and thermal dissipations will decrease leading to smaller cavity damping.

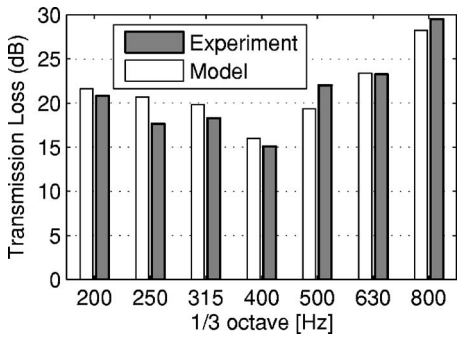

FIG. 19. Comparison with experiment—Double aluminum panel (Lx=0.96 m, Lz=1.5 m), 2 and 1.5 mm thickness, separated by 3 cm of air, centered on point X=6 m, Y=0 m, Z=1.75 m—Room dimensions: lx=11.5 m, ly=8.69 m, lz=4.03 m—Patch size: ΔX=0.08 m, ΔZ=0.074 m—Source at: Xs=2 m, Ys=4 m, Zs=1 m, amplitude: S_0=2—cutoff frequency: 187 Hz—structural damping: 0.06—fluid damping: 0.035.

XI. CONCLUSIONS

A patch-mobility method is presented in this paper and is used to predict transmission loss of finite double panels. Excitation is modeled with blocked patch pressures that are calculated from the source room response, taking thus into account source room dimensions, absorption, excitation position, and panel location. Calculation time is, hence, considerably reduced compared to classical plane waves summation technique to represent reverberant field. Moreover, the substructural approach used in the patch-mobility method enables to characterize each subsystem separately before coupling. Another powerful numerical aspect of this method is the mesh criterion in $\lambda_s/2$ that is very large compared to standard finite element analysis mesh criterion. The patch-mobility model and finite element model give the same results when comparing transmission loss of double panels. However, the patch-mobility method enables to study higher frequencies. Finally, a good agreement is found with experimental measurements realized on a double aluminium panel.

APPENDIX A: CAVITY MOBILITY

After having multiplied the Helmoltz Eq. (32) by the mode shape $\psi_p(M)$, the integration over the volume Ω yields to

$$\int_\Omega [\Delta P(M) + k^{*2} P(M)]\psi_p(M) d\Omega = 0. \tag{A1}$$

Using Green's formulas gives

$$\int_\Omega [\Delta \psi_p(M) + k^{*2}\psi_p(M)]P(M) dM - \int_{\partial\Omega} \left[\psi_p(Q) \frac{\partial P(Q)}{\partial n} - P(Q) \frac{\partial \psi_p(Q)}{\partial n} \right] dQ = 0. \tag{A2}$$

Conditions over boundary surface $\partial\Omega$ are defined over different surfaces: $\partial P(Q)/\partial n = -j\rho\omega V_n(Q)$ $\forall Q \in \partial\Omega_+ \partial P(Q)/\partial n = 0$ $\forall Q \in \partial\Omega_- \partial\psi_p(Q)/\partial n = 0 \forall Q \in \partial\Omega$.

Equation (A2) becomes

$$\int_\Omega [\Delta \psi_p(M) + k^{*2}\psi_p(M)]P(M) dM = \int_{\partial\Omega_+} \{\psi_p(Q)[-j\rho\omega V_n(Q)]\} dQ. \tag{A3}$$

Pressure is then replaced by its modal expansion (33):

$$\int_\Omega [\Delta \psi_p(M) + k^{*2}\psi_p(M)] \sum_m [a_m \psi_m(M)] dM = \int_{\partial\Omega_+} \{\psi_p(Q)[-j\rho\omega V_n(Q)]\} dQ. \tag{A4}$$

Thanks to modes orthogonality, this expression is simplified

$$\int_{\Omega}[-k_p^2\psi_p(M)+k^{*2}\psi_p(M)]a_p\psi_p(M)dM$$

$$=\int_{\partial\Omega_+}\{\psi_p(Q)[-j\rho\omega V_n(Q)]\}dQ. \quad \text{(A5)}$$

Mode amplitude a_p is then obtained

$$a_p=\frac{\int_{\partial\Omega_+}\{\psi_p(Q)[-j\rho\omega V_n(Q)]\}dQ}{(k^{*2}-k_p^2)N_p} \quad \text{(A6)}$$

with $N_p=\int_{\Omega}\psi_p^2(M)dM$.

Using this modal amplitude into Eq. (33) enables to find the pressure radiated at point M:

$$P(M)=\sum_p\left(\frac{\int_{\partial\Omega_+}\{\psi_p(Q)[-j\rho\omega V_n(Q)]\}dQ}{(k^{*2}-k_p^2)N_p}\psi_p(M)\right). \quad \text{(A7)}$$

APPENDIX B: RADIATION IMPEDANCE

Rayleigh's integral (B1) is used to calculate the radiated pressure of the panel. Two integrals can be written depending on the observation point location. Indeed, for a point located on the boundary surface, the Green's function singularity needs to be avoided, through the calculation of Cauchy's principal value integral (B2):

$$P(M_0)=\int_{\partial\Omega_+}\left[j\rho\omega V_n(Q)\frac{\exp(-jk\|QM_0\|)}{2\pi\|QM_0\|}\right]dQ \quad \forall M_0\in Q, \quad \text{(B1)}$$

$$P(Q_0)=\oint_{\partial\Omega_+}\left[j\rho\omega V_n(Q)\frac{\exp(-jk\|QQ_0\|)}{2\pi\|QQ_0\|}\right]dQ \quad \forall Q_0\in\partial Q. \quad \text{(B2)}$$

The vibrating surface $\partial\Omega_+$ is separated in patches S_i leading to equation

$$P(Q_0)=\sum_{j=1,j\neq i}^{N}\int_{S_j}\left[j\rho\omega V_n(Q_j)\frac{\exp(-jk\|Q_jM_0\|)}{2\pi\|Q_jM_0\|}\right]dQ_j+\oint_{S_i}\left[j\rho\omega V_n(Q_i)\frac{\exp(-jk\|Q_iQ_0\|)}{2\pi\|Q_iQ_0\|}\right]dQ_i. \quad \text{(B3)}$$

Let us introduce the distance d_{ij} between two patch centers. If the patch dimensions are small, the integral can be approximated by the value at the central point times the patch area. Moreover, the velocity $V_n(Q)$ being approximated by a uniform value over the patch, it can be put out of the integral. These assumptions lead to the classical approximation of the integral

$$\int_{S_j}\left[j\rho\omega V_n(Q_j)\frac{\exp(-jk\|Q_jM_0\|)}{2\pi\|Q_jM_0\|}\right]dQ_j=\frac{1}{2\pi}\rho_0j\omega\langle V\rangle_j\frac{\exp^{-jkd_{ij}}}{d_{ij}}S_j, \quad \text{(B4)}$$

where d_{ij} is the distance between two patches.

This approximation is valid for small enough patch surface, in general a discretization based on the standard $\lambda/6$ criterion is sufficient.

The use of cylindrical coordinates enables us to calculate Cauchy's principal value of the integral by considering a circular patch having the same surface as the original one. The result is immediate

$$\oint_{S_i}\left[j\rho\omega V_n(Q_i)\frac{\exp(-jk\|Q_iQ_0\|)}{2\pi\|Q_iQ_0\|}\right]dQ_i=\rho_0c\langle V\rangle_i[1-\exp^{-jka}]. \quad \text{(B5)}$$

[1] L. Cremer, "Theorie der schalldämmung dünner bei schragen einfall (theory of sound absorption of thin walls)," Akust. Z. **7**, 81–104 (1942).
[2] A. London, "Transmission of reverberant sound through single walls," J. Res. Natl. Bur. Stand. **42**, 605 (1949).
[3] A. London, "Transmission of reverberant sound through double walls," J. Acoust. Soc. Am. **22**, 270–279 (1950).
[4] T. Vogel, "Sur les vibrations de certains systèmes élastiques dans un champ sonore (vibrations of elastic systems in an acoustic field)," Ph.D. thesis, Marseille, 1947.
[5] M. Battacharya and M. Crocker, "Forced vibration of a panel and radiation of sound into room," Acustica **22**, 275–294 (1970).
[6] R. Guy and M. Battacharya, "The transmission of sound through a cavity-backed finite plate," J. Sound Vib. **27**, 207–223 (1973).
[7] K. Mulholland and R. Lyon, "Sound insulation at low frequencies," J. Acoust. Soc. Am. **54**, 867–878 (1973).
[8] L. Beranek, *Noise Reduction* (McGraw-Hill, NY, 1960).
[9] F. Fahy, *Sound and Structural Vibration: Radiation Transmission and Response* (Academic, New York, 1985).
[10] K. Ballagh, "Accuracy of prediction methods for sound transmission loss," Internoise Proceedings, 2004 (INCE, Ames, IA).
[11] N. Atalla and R. Bernhard, "Review of numerical solutions for low-frequency structural-acoustic problems," Appl. Acoust. **43**, 271–294 (1994).
[12] L. Gagliardini, J. Rolland, and J. Guyader, "The use of a functional basis to calculate acoustic transmission between rooms," J. Sound Vib. **145**, 457–478 (1991).
[13] J. Guyader and B. Laulagnet, "Structural acoustic radiation prediction: Expanding the vibratory response on a functional basis," Appl. Acoust. **43**, 247–269 (1994).
[14] A. Price and M. Crocker, "Sound transmission through double panels using statistical energy analysis," J. Acoust. Soc. Am. **47**, 683–693 (1970).
[15] R. Craik and R. Smith, "Sound transmission through leaf lightweight partitions—Part i: Airborne sound," Appl. Acoust. **61**, 223–245 (2000).
[16] W. Kropp and E. Rebillard, "On the air-borne sound insulation of double wall constructions," Acust. Acta Acust. 85, 707–720 (1999).
[17] J. Guyader, "Transparence acoustique de plaques multicouhes orthotropes, viscoélastiques, finies (acoustic transparency of multilayered orthotropic viscoplastic plates)," Ph.D. thesis, Université Claude Bernard, Lyon I, 1977.
[18] J. Guyader and C. Lesueur, "Acoustic transmission through orthotropic multilayered plates, part ii: Transmission loss," J. Sound Vib. **58**, 69–86 (1978).
[19] J. Guyader and C. Lesueur, "Transmission of reverberant sound through orthotropic viscoelastic multilayered plates," J. Sound Vib. **70**, 319–332 (1980).
[20] E. Nilsson and A. Nilsson, "Prediction and measurement of some dynamic properties of sandwich structures with honeycomb and foam cores," J. Sound Vib. **251**, 409–430 (2002).
[21] R. Panneton and N. Atalla, "An efficient finite element scheme for solving the three dimensional poroelasticity problem in acoustics," J. Acoust. Soc. Am. **101**, 3287–3298 (1997).
[22] N. Atalla, M. A. Hamdi, and R. Panneton, "Enhanced weak integral formulation for the mixed (u, p) poroelastic equations," J. Acoust. Soc. Am. **109**, 3065–3068 (2001).
[23] R. Panneton and N. Atalla, "Numerical prediction of sound transmission through finite multilayer systems with poroelastic materials," J. Acoust. Soc. Am. **100**, 346–354 (1996).

[24]F. Spronck, "Transparence au son des parois minces viscoélastiques finies et infinies, simples ou multiples (sound transparency of thin infinite viscoelastic plates)," Ph.D. thesis, Marseille, 1971.
[25]J. Coyette, G. Lielens, M. Robbé, and P. Neple, "An efficient method for evaluating diffuse field joint acceptance functions for cylindrical and truncated conical geometries," J. Acoust. Soc. Am. **117**, 1009–1019 (2005).
[26]J. O'Hara, "Mechanical impedance and mobility concepts," J. Acoust. Soc. Am. **41**, 1180–1184 (1967).
[27]B. Petersson, "A thin-plate model for the moment mobility at the intersection of two perpendicular plates," J. Sound Vib. **108**, 417–485 (1986).
[28]A. T. Moorhouse, "A dimensionless mobility formulation for evaluation of force and moment excitation of structures," J. Acoust. Soc. Am. **112**, 972–980 (2002).
[29]A. T. Moorhouse and B. Gibbs, "Calculation of the mean and maximum mobility for concrete floors," Appl. Acoust. **45**, 227–245 (1995).
[30]S. Naji, "Etude des transmissions vibratoires par une méthode de mobilité mixte dans les assemblages par surface (study on vibration transmissions with a mobility method)," Ph.D. thesis, Université Claude Bernard Lyon I, 1993.
[31]G. Orefice, C. Cacciolati, and J. Guyader, "The energy mobility," J. Sound Vib. **254**, 269–295 (2002).
[32]M. Ouisse, L. Maxit, C. Cacciolati, and J. Guyader, "Patch transfer functions as a tool to couple linear acoustics problems," J. Vibr. Acoust. **127**, 458–466 (2005).
[33]P. Fausti, R. Pompoli, and R. S. Smith, "An intercomparison of laboratory measurements of airborne sound insulation of lightweight plasterboard walls," Build. Acoust. **6**, 127–140 (1999).
[34]J. Brunskog, "The influence of finite cavities on the sound insulation of double-plate structures," J. Acoust. Soc. Am. **117**, 3727–3739 (2005).